Comparison of Regional Climate Model Performances for Different Types of Heat Waves over South Korea

Donghyuck Yoon,[a] Dong-Hyun Cha,[a] Myong-In Lee,[a] Ki-Hong Min,[b] Sang-Yoon Jun,[c] and Yonghan Choi[c]

[a] *Department of Urban and Environmental Engineering, Ulsan National Institute of Science and Technology, Ulsan, South Korea*
[b] *Department of Astronomy and Atmospheric Sciences, Kyungpook National University, Daegu, South Korea*
[c] *Unit of Arctic Sea-Ice Prediction, Korea Polar Research Institute, Incheon, South Korea*

ABSTRACT: South Korea's heat wave events over 39 years (1980–2018) were defined by spatiotemporal criteria, and their quantitative characteristics were analyzed. The duration and intensity of these events ranked highest in 2016 and 2018. An examination of synoptic conditions of heat wave events in 2016 and 2018 based on a reanalysis dataset revealed a positive anomaly of 500-hPa geopotential height, which could have induced warm conditions over the Korean Peninsula in both years. However, a difference prevailed in that there was a blocking high over the Kamchatka Peninsula and a continental thermal high over northern China in 2016, while the expansion of the western North Pacific subtropical high was mainly associated with 2018 heat wave events. Numerical experiments using the Weather Research and Forecasting (WRF) Model were conducted to 1) evaluate how distinct meteorological characteristics of heat wave events in 2016 and 2018 were reproduced by the model, and 2) investigate how they affect extreme temperature events. Typical synoptic features of the 2016 heat wave events (i.e., Kamchatka blocking and continental thermal high) were not captured well by the WRF Model, while those of 2018 were reasonably reproduced. On the contrary, the heat wave event during late August 2016 related to the Kamchatka blocking high was realistically simulated when the blocking was artificially sustained by applying spectral nudging. In conclusion, the existence of a blocking high over the Kamchatka region (i.e., northern Pacific region) is an important feature to accurately predict long-lasting heat waves in East Asia.

KEYWORDS: Asia; Extreme events; Numerical analysis/modeling; Regional models; Blocking

1. Introduction

Due to the increased frequency of severe heat waves, more attention has been paid to them. The heat waves in the summer of 2003 in Europe, for example, caused ~35 000 deaths; it was recorded as the hottest summer over the last 500 years (Larsen 2003; Luterbacher et al. 2004; IPCC 2013). In 2010, Russia and eastern Europe were exposed to an extreme heat wave wherein the temperature exceeded the 1970–99 mean by 10°C—a standard deviation of >4°C (Barriopedro et al. 2011). In addition, severe heat waves have been reported globally (e.g., North America, 2012; Australia, 2012–13; Northern Hemisphere, 2018). Many studies point out that heat waves will be more intense, frequent, and prolonged in the twenty-first century (Meehl and Tebaldi 2004; Coumou et al. 2013). East Asia, including eastern China, Japan, and the Korean Peninsula, has also been experiencing extreme temperatures lately (Nakai et al. 1999; Kysely and Kim 2009; Sun et al. 2014). South Korea, for instance, suffered from extreme heat waves in 1994, 2013, 2016, and 2018 (Kysely and Kim 2009; Yeh et al. 2018; Im et al. 2019; S.-K. Min et al. 2020). In particular, the heat waves of 2016 and 2018 have been recorded as the most prolonged and harmful ones ever (Lee et al. 2020). According to the Korea Centers for Disease Control and Prevention, there were 2125 people with heat-related diseases in 2016 in South Korea due to a heat wave lasting over 22 days; this record was broken in 2018 with 4526

people. Despite a recent increase in damage caused by the heat waves in South Korea, their detailed mechanism has not been well understood. Therefore, an accurate prediction of heat wave characteristics with an understanding of their mechanisms is required to reduce related damage.

The presence of an anticyclonic circulation over the midlatitude region in summer is considered one of the leading causes that induces warm temperatures by producing low cloudiness, clear skies, and warm advection (Black et al. 2004; Meehl and Tebaldi 2004; Fischer et al. 2007). In the case of the East Asian summer monsoon region (East China, South Korea, and Japan), the expansion of the western North Pacific subtropical high (WNPSH) significantly influences the summer heat wave. Ding et al. (2010) indicated that an enhanced WNPSH in terms of anticyclonic anomalies of the 500-hPa geopotential height centered over the Yellow Sea and the Korean Peninsula results in anomalously high frequencies of heat wave days in East China. Yoon et al. (2018) mentioned that the heat waves affecting South Korea were divided into three categories based on spatial distributions of maximum surface air temperature (i.e., entire Korea type, northwestern Korea type, and southeastern Korea type) and were influenced by the intensity and location of the WNPSH as a synoptic factor. In addition, recent studies have been noting the influence of large-scale atmospheric circulation patterns associated with heat waves in South Korea. Lee and Lee (2016) demonstrated the connection between interannual variability of the frequency of heat waves in South Korea and large-scale atmospheric patterns, such as the Rossby wave train, which are

initiated by a tropical heat source over southern China. They showed that the 500-hPa geopotential height anomaly shows a positive maximum over the Korean Peninsula and Japan whose pattern extends zonally. This spatial pattern of midlevel geopotential height that correlates with South Korea's heat waves has also been emphasized in other studies (M.-K. Kim et al. 2019; Yeo et al. 2019; Choi et al. 2020).

In terms of synoptic-scale atmospheric circulation patterns, a blocking high over the Kamchatka Peninsula and continental thermal high over northeastern China could be other significant contributors toward a heat wave in South Korea. According to Yeh et al. (2018), an anomalously high midlevel geopotential height over Mongolia, as well as WNPSH, played a significant role in inducing the August 2016 heat wave. They suggested that the hot air mass associated with continental thermal high over northern China was advected to the Korean Peninsula in August 2016 and this system was continued by the blocking over the Kamchatka Peninsula. Furthermore, on comparison with previous heat waves, the geopotential height over the Kamchatka Peninsula in August 2016 was the highest since 1979, causing atmospheric blocking downstream of the Korean Peninsula. K. H. Min et al. (2020) examined widespread blocking events over the northern Pacific Ocean and Asia during the South Korean heat waves in 1994, 2013, and 2016, using blocking indices. During heat waves, the blocks were large and extended to much of the North Pacific and Asia, indicating that the atmospheric flow in the region became stationary. Both studies revealed the existence of blocking events over the North Pacific during heat waves; however, they are limited in that they did not introduce a detailed mechanism of how anticyclones over the region affect extreme temperatures in South Korea using a numerical weather prediction model.

The Korea Meteorological Administration (KMA) established a heat wave forecasting system and has issued official advisories/warnings since 2008. However, the 2016 heat wave lasted longer than they expected, as high temperatures were underestimated in the medium-range forecast system. Conversely, the KMA predicted the 2018 heat wave relatively accurately, although its intensity and duration were more significant. This may be due to the different synoptic characteristics of the 2016 and 2018 heat waves. Matsueda (2011) reported that low predictability of Euro-Russian blocking in the summer of 2010 could be related to the failure in predicting heat waves associated with the mature blocking in early August; most of the medium-range ensemble forecasts predicted decay of the blocking earlier than the observations in the research. Thus, an investigation of the blocking effect in summer on heat waves and the evaluation of simulated blocking in a numerical model are required to predict heat waves accurately.

Regional climate models (RCMs) are useful in analyzing mechanisms of extreme climate events as they can reproduce such events more clearly than global climate models using higher-resolution grids. Previous studies have used RCMs to examine the causes and mechanisms of high-impact weather and climate such as floods, droughts, heat waves, and heavy snowfalls (Giorgi and Marinucci 1996; Xue et al. 2001; Hong and Kalnay 2002; Cha et al. 2011a; Yoon et al. 2018; J. Kim

et al. 2019). For instance, Yoon et al. (2018) suggested an impact of local factors on 2015 heat waves over South Korea by using a high-resolution Weather Research and Forecasting (WRF) Model. However, few studies use RCMs to investigate the larger-scale mechanisms of the recent heat waves over South Korea. Thus, we adopted the WRF Model to effectively simulate atmospheric processes of the 2016 and 2018 heat wave events by reproducing synoptic factors (e.g., WNPSH, Kamchatka blocking), which are dominant components for characterizing South Korean heat waves. Especially, the spectral nudging (SN) technique (Miguez-Macho et al. 2004) was employed to investigate the association between 2016 heat wave events and Kamchatka blocking.

This study aims to 1) evaluate how distinct characteristics of heat wave events in 2016 and 2018 are reproduced in the model and 2) investigate how they affect extreme temperature events, based on comparing the meteorological characteristics of those events. The observational characteristics of heat wave events of 2016 and 2018 were examined based on a station and reanalysis dataset. Then, the simulated results of the WRF Model, primarily focused on the anomalous anticyclone patterns over East Asia, were evaluated by applying the SN method. The data and methods are represented in section 2. Section 3 includes the detailed result and interpretation. The summary and discussion are given in section 4.

2. Data and method

a. Characteristics of heat wave events

1) DEFINING HEAT WAVE EVENTS

The procedure for defining heat wave events, which includes deciding the criteria, mainly follows previous studies (Yoon et al. 2018, 2020). South Korea's heat wave events over 39 years (1980–2018) were defined by considering three spatiotemporal criteria: temperature threshold, spatial continuity, and temporal continuity. Through this process, the heat wave periods that vary by each grid can be unified in consideration of spatiotemporal continuity. First, daily "hot" stations were defined as those where the daily maximum surface air temperature (TMAX), in the KMA Automated Surface Observing System (ASOS) station data, exceeded the threshold value T. The threshold value T was decided based on the official KMA criteria for a heat wave warning. Then, isolated hot stations were eliminated, if a given station for which the ratio of the number of hot stations to the total number of stations within a given distance D was smaller than a specific value α. The D and α values were selected according to the suggestion of Yoon et al. (2020), which was reasonably adjusted on the analysis region. As a temporal gap between heat wave days was not considered when defining a single heat wave event, the ratio of overlapping hot stations between 2 days d was calculated if the similarity ratio between consecutive days exceeded a specific threshold value S. The similarity ratio of the station distribution is determined as the ratio of the number of all hot stations and number of overlapped hot stations in both time steps (Yoon et al. 2018). The criteria for defining heat wave events are described in Table 1.

TABLE 1. Criteria for defining heat waves.

T	D	α	d	S
33°C	0.75°	0.6	2 days	30%

2) HEAT WAVE INDICES

Heat wave characteristics such as frequency, duration, and intensity can be quantified by applying several indices (Perkins and Alexander 2013; Wang et al. 2019). Here, four heat wave indices were used to investigate the quantitative characteristics of heat wave events over South Korea: heat wave total intensity (HWTI/HWTI$_G$), and heat wave intensity (HWI/HWI$_G$). They are defined as

$$\text{HWTI} = \sum_{i=1}^{D} \sum_{j=1}^{M} (\text{TMAX}_{ij} - 33), \quad \text{where } \text{TMAX}_{ij} \geq 33\,°\text{C}, \quad (1)$$

$$\text{HWI} = \frac{\sum_{i=1}^{D} \sum_{j=1}^{M} (\text{TMAX}_{ij} - 33)}{D}, \quad \text{where } \text{TMAX}_{ij} \geq 33\,°\text{C}, \quad (2)$$

$$\text{HWTI}_G = \sum_{i=1}^{D} (\text{TMAX}_i - 33), \quad \text{where } \text{TMAX}_i \geq 33°\text{C, and} \quad (3)$$

$$\text{HWI}_G = \frac{\sum_{i=1}^{D} (\text{TMAX}_i - 33)}{D}, \quad \text{where } \text{TMAX}_i \geq 33°\text{C}, \quad (4)$$

where TMAX$_{ij}$ implies daily maximum surface air temperature at day i and grid point j; D is the duration of each heat wave event (number of days), here denoted as heat wave days (HWDs); and M represents the number of grids over South Korea. The value of 33°C in HWTI and HWI corresponds to the threshold temperature defining heat wave events. All heat wave indices represent the quantitative characteristic of each heat wave event, but HWTI and HWI differ in that HWTI describes both the duration and intensity of heat waves, whereas HWI describes only the intensity for each day during a heat wave event. In addition, HWTI$_G$ and HWI$_G$, which were calculated without a summation of the total grid, were also defined to analyze the heat wave characteristics of each grid.

3) DATA

TMAX data from the ASOS for 98 stations of the KMA in South Korea were used to define heat wave events over 39 years (1980–2018). The spatial distribution of ASOS stations is shown in Fig. 1 as black dots. The TMAX data from observation stations were converted to grid data using Barnes scheme (Barnes 1964) to help interpolate missing points while calculating heat wave indices. The horizontal resolution of gridded ASOS data is 0.25° × 0.25° over South Korea; the total number of grids covering South Korea is 29 × 29, and the number of grids on the land surface, except the ocean, is 216. Temporal mean synoptic conditions for the heat wave events, that is, the geopotential height and its anomaly, were represented by employing the six-hourly ERA-Interim reanalysis (ERAIN) data (Dee et al. 2011) from 1980 to 2018.

b. Numerical experiments

1) DATA AND MODEL CONFIGURATIONS

The WRF Model, version 3.9.1 (Skamarock et al. 2005), was used for numerical modeling. The simulation was conducted for 2016 and 2018, beginning at 0000 UTC 1 June 2016 (2018), and ran for three months, until 0000 UTC 1 September 2016
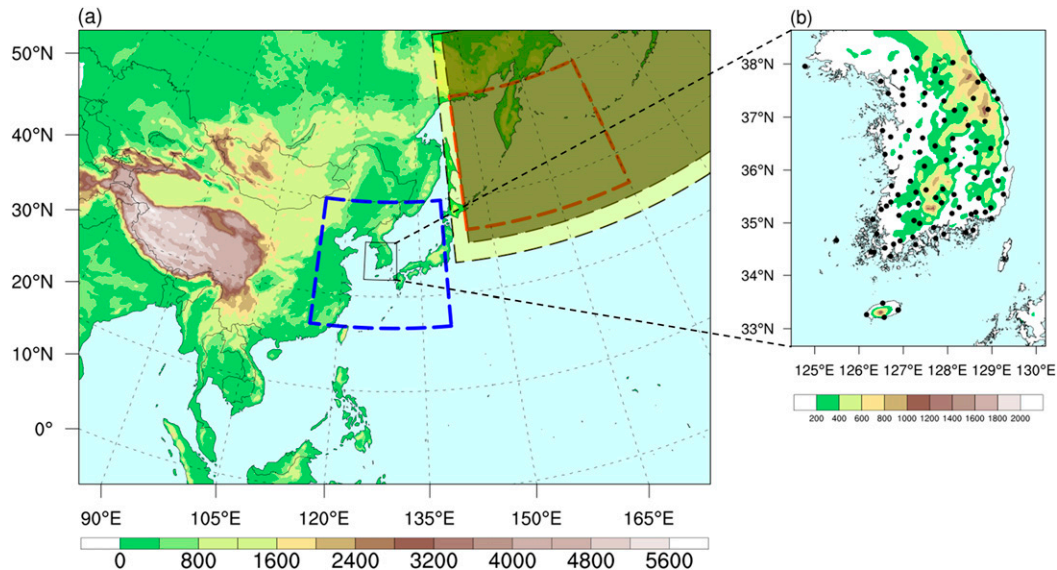

FIG. 1. (a) Topographical height (m) over domain 1 and (b) domain 2 with locations of ASOS over South Korea (black dots). Red and blue dashed lines indicate the Kamchatka Peninsula (40°–60°N, 145°E–180°) and the Korean Peninsula (25°–45°N, 115°–140°E) areas, respectively. Black and yellow shaded areas indicate the spectral nudging region.

TABLE 2. Model configurations with settings for the SN experiment.

Model	WRF Model, version 3.9.1	
Domain (horizontal resolution)	Domain 1	Domain 2
	321×446 (25 km)	131×111 (5 km)
Simulation period	0000 UTC 1 Jun 2016 (2018)–0000 UTC 1 Sep 2016 (2018)	
Initial/boundary condition	Final analysis data, six-hourly, 1° horizontal resolution	
Microphysics	WSM6	
Cumulus	Kain–Fritsch	—
Radiation: Shortwave	RRTMG	
Radiation: Longwave	RRTMG	
Planetary boundary layer	YSU	
Land surface model	Unified Noah Land Surface Model	

SN experiment setting			
Wavelength (km)	Coefficient (s^{-1})	Variables	Nudging interval (h)
~1000	0.0003	U, V, T	6

(2018). The first month of the simulation period was considered as a spinup time; the analysis period was considered from 0000 UTC 1 July 2016 (2018) to 0000 UTC 1 September 2016 (2018). Simulations were performed using a two-way nesting system with two model domains, with 25- and 5-km horizontal resolutions. Every domain covered East Asia while domain in particular focuses on South Korea (Fig. 1). All runs used the six-hourly National Centers for Environmental Prediction Global Data Assimilation System Final Analysis (FNL) data on $1° \times 1°$ horizontal resolution, as the initial and lateral boundary conditions. Optimal Interpolation Sea Surface Temperature data (Reynolds et al. 2007) were prescribed as a lower boundary, coming into force every six hours. FNL data were used for the model evaluation to examine a simulated performance of the synoptic variables. Hourly surface air temperature data from KMA ASOS were also compared with the model results, which were bilinearly interpolated from the nearest grids for comparison with station data. Physical parameterization schemes were used to model subgrid-scale events in the WRF experiments. The model includes the WRF single-moment 6-class microphysics scheme (Hong and Lim 2006) while Kain–Fritsch cumulus parameterization (Kain 2004) was applied only for domain 1. For parameterizing the planetary boundary layer, the Yonsei University scheme (Hong et al. 2006) was employed. The longwave and shortwave radiation scheme from the Rapid Radiative Transfer Model for Global Circulation Model scheme (Iacono et al. 2008) was used. The Unified Noah Land surface Model (Tewari et al. 2004) was employed to model land surface and soil conditions; it contains four soil layers with thicknesses of 10, 30, 60, and 100 cm. A detailed configuration of the numerical experiments is included in Table 2.

2) SN

RCMs have an issue of lateral boundary conditions in simulating long-term regional climate, even though they are useful for simulating or predicting regional climates. Therefore, many studies suggest that the SN technique reduces systematic errors in regional climate simulations, especially over East Asia and the western North Pacific area (Miguez-Macho et al. 2004; Cha

and Lee 2009; Cha et al. 2011b, 2016; Moon et al. 2018; Wang et al. 2019). SN, in numerical modeling, helps provide large-scale forcing data into a regional model from its lateral boundaries to the interior (von Storch et al. 2000). Large-scale waves longer than the cutoff wavelength are dismantled from lateral boundary data and combined with the entire regional model field in SN process. Thus, RCM produces its dynamics at a regional scale, while it retains large-scale characteristics of boundary forcing. Here, two experiments were conducted to investigate the effects of peculiar climate characteristics, chiefly Kamchatka blocking, on heat wave events over South Korea: 1) a no-spectral nudging (NOSN) experiment, that is, without applying spectral nudging; 2) an SN experiment adopted only over the Kamchatka Peninsula area (black dashed lines in Fig. 1). Large-scale forcing data (i.e., FNL) was carried out only over the Kamchatka area (black shaded area in Fig. 1) in the SN experiment as we presumed that the WRF Model could not capture extreme heat waves of 2016, which was significantly influenced by the Kamchatka blocking. Note that applying spectral nudging over the particular region was not suggested as a method or technique to improve the simulation performance of the numerical model in this study. Spectral nudging was used only as a way to reproduce the blocking over the Kamchatka area. To reduce the inconsistency between the nudging area and the outer boundary, a buffer zone was set around the southern and western boundaries of the nudging area (yellow shaded area in Fig. 1). The grid number of the buffer zone is eight, corresponding to ~200 km, and the nudging coefficient was linearly reduced from 80% to 20%, as it got farther away from the nudging area. The reduced nudging coefficient η within the buffer zone is a function of horizontal grids given by

$$\eta(k) = \eta_{\text{org}}(1 - 0.1k) \begin{cases} k = i, & \text{where } i = 2n \\ k = i + 1, & \text{where } i = 2n - 1, \end{cases} \quad (5)$$

where i is a grid number ranging from 1 to 8, and η_{org} is an original nudging coefficient. Waves of u-component wind, v-component wind, and potential temperature, whose wavelengths were >1000 km, were nudged with a nudging coefficient of $0.0003\,s^{-1}$. SN was applied across the entire vertical
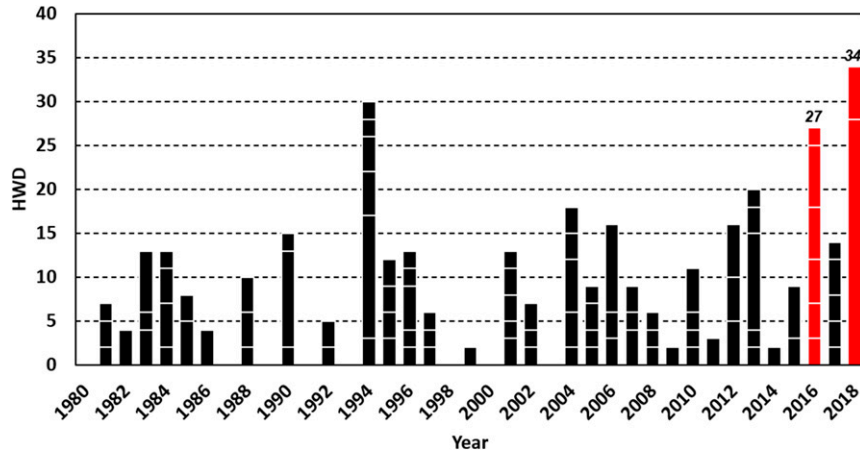
FIG. 2. Time series of annual HWDs during 1980–2018. The bars separated with white dashed lines indicate each heat wave.

levels. Previous studies have shown that a two-way nesting technique is useful tool for simulating atmospheric features (Harris and Durran 2010; Bowden et al. 2012). We consider that the spectral nudging technique used in this study is not much different from the two-way nesting method in that the parent domain and nested domain interacts integrated results with each other. Since this study was not aimed to improve the simulation performance of the RCM, it was determined that the use of spectral nudging as a way of reproducing the blocking was appropriate.

3. Results

a. Characteristics of 2016 and 2018 heat wave events

Based on the definition of heat wave events, 97 such events in South Korea with a total duration of 357 days were identified during the 39-yr period (1980–2018). Figure 2 shows the time series of annually accumulated HWDs for 1980–2018. The total HWDs of heat wave events in 2016 and 2018 were 27 and 34 days, ranking third and first, respectively, among those of the last 39 years. Six heat wave events occurred over the 27 days of 2016, whereas only two events occurred over the 34 days of 2018. Also, in terms of the intensity of the heat wave events, those of 2016 and 2018 were noticeable. Table 3 describes the heat wave indices for the heat wave events of 2016 and 2018; rankings of each event based on HWTI and HWI among 97 heat wave events during 1980–2018 are also shown. The most severe heat wave in the summer of 2016 was from 10 to 15 August (2016D); previous studies also mention this period to be the most intense one, in terms of maximum temperature (Yeh et al. 2018; K. H. Min et al. 2020). The HWTI and HWI over these six days were 1587.2° and 264.5°C, respectively, being the seventh and fifth highest out of the 97 heat waves, respectively. Both heat wave events of 2018 were significantly severe, particularly the one that lasted 28 days from 13 July to 9 August (2018A), which had the highest HWTI among all events. The heat wave events of 2018 from 10 to 15 August (2018B) also ranked high; fifth and fourth, based on

HWTI and HWI, respectively. Several other extreme heat wave events that existed during 1980–2018 (e.g., 1984, 1990, 1994, and 2013); however, those of 2016 and 2018 were the most severe ones since the 2000s (not shown). Especially, the year having the second-longest HWD was 1994, indicated in many previous studies to have had one of the most extreme heat waves, causing extensive damage over South Korea (Kysely and Kim 2009; Kim et al. 2015; Choi and Lee 2019). However, the 1994 heat wave events were excluded from this study because various research suggested the main factor that affected those events was the expansion of WNPSH, as with 2018 cases (Lee and Lee 2016; Yeo et al. 2019; Yoon et al. 2020). In addition, as mentioned in the introduction section, the motivation of this study was to understand the different predictabilities of the KMA forecasting system between heat wave events in 2016 and 2018. The heat waves in 2016 lasted longer than they expected, while the KMA predicted the heat waves in 2018 relatively accurately despite stronger intensity and longer duration than those in 2016. We assumed that it was due to the difference in synoptic factors between 2016 and 2018. Because the KMA's heat wave warning system using their own forecasting system began in 2008, the forecast performance of the heat waves in 1994 could not be compared.

The spatial distributions of $HWTI_G$ and HWI_G for the heat wave events of 2016 and 2018 are represented in Figs. 3 and 4, respectively. As the duration of a heat wave event is included while calculating $HWTI_G$, only 2018A, which was exceptionally long-lasting as compared to others, had a distinctive $HWTI_G$ spatial pattern (Fig. 3); during this period, $HWTI_G$ had a maximum value over the southeastern region of South Korea; a high $HWTI_G$ value was also observed over the northwestern region of South Korea. This spatial distribution of $HWTI_G$ in 2018 corroborated the results of Im et al. (2019); they mentioned that the distinct behavior of TMAX in 2018 mainly represented a statistical analogy of the distribution pattern expected under 3°C global warming based on finescale climate projections. Moreover, the population of South Korea is concentrated in these two regions, and the mortality rate of

TABLE 3. HWD, HWTI, and HWI for the heat waves of 2016 and 2018.

Year	Date	HWD (days)	HWTI (°C)	Ranking (HWTI)	HWI (°C)	Ranking (HWI)
2016	26–28 Jul	3	128.6	64	42.9	73
	29 Jul–1 Aug	4	318.2	33	79.5	42
	4–8 Aug	5	745.7	18	149.1	19
	10–15 Aug	6	1587.2	7	264.5	5
	16–22 Aug	7	792.5	17	113.2	30
	24–25 Aug	2	165.3	51	82.7	39
2018	13 Jul–9 Aug	28	7904.3	1	282.3	3
	10–15 Aug	6	1658.4	5	276.4	4

large cities within these regions tends to be higher with more intense and longer-lasting heat waves (Son et al. 2012). This implies that this regional distribution of a high $HWTI_G$ in 2018 could have caused more casualties as compared to that of other heat wave events. As HWI_G is standardized by the HWD of the

event, spatial distributions of HWI_G for the other heat wave events become comparable with 2018A, although that of 2018A remains the most extreme over the northwestern and southeastern regions (Fig. 4). In particular, the HWI_G of 2016D and 2018B had significant distributions over South
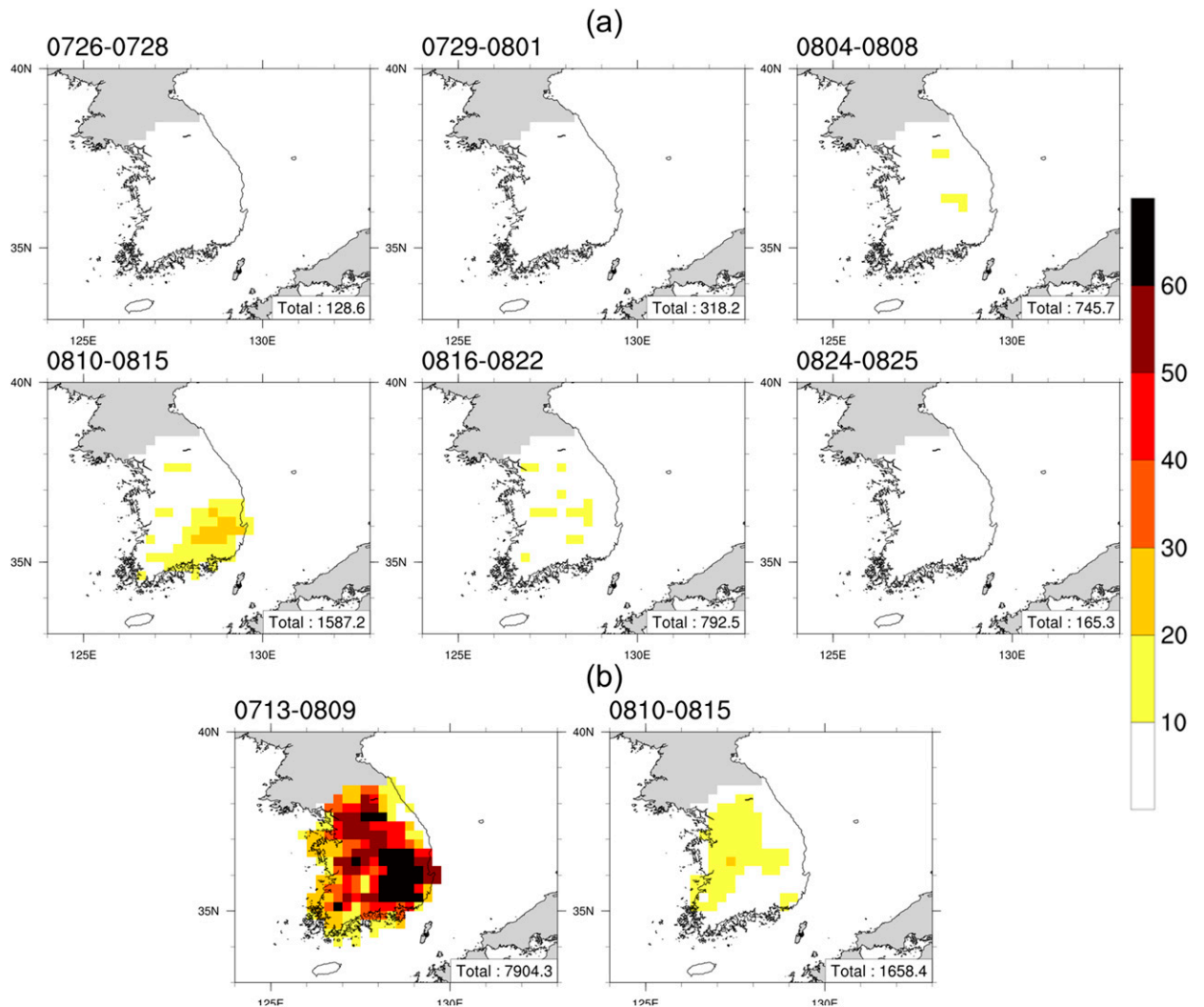

FIG. 3. Spatial distributions of $HWTI_G$ (°C) for the heat waves in (a) 2016 and (b) 2018. The numbers in the bottom-right boxes indicate the HWTI during each period.
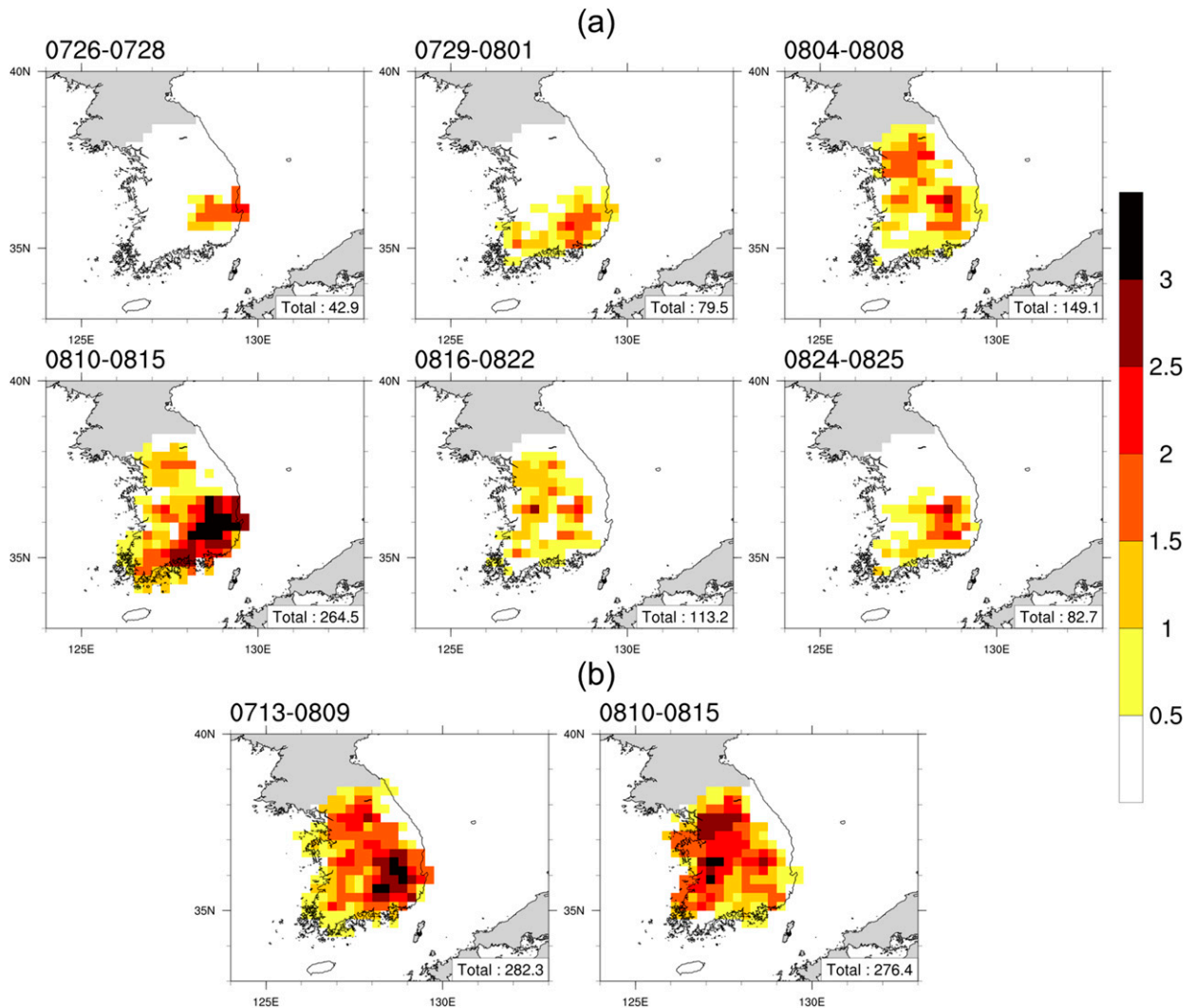
FIG. 4. Spatial distributions of HWI$_G$ (°C) for the heat waves in (a) 2016 and (b) 2018. The numbers in the bottom-right boxes indicate the HWI during each period.

Korea. As with 2018A, 2016D had the highest HWI$_G$ over the southeastern and the northwestern regions. The HWI$_G$ over those regions was also apparent during 4–8 August 16 (2016C) and 16–22 August 2016 (2016E), but less severe. However, 2016E was unusual, as such events rarely occurred, climatologically, during similar historical periods, and lasted longer as compared to 2016C and 2016D; as heat wave events occurred most frequently, and intensely during similar historical periods (Lee and Lee 2016; Xu et al. 2019). A maximum HWI$_G$ also appeared over the same area in 2018B. Consequently, the spatial patterns of heat wave indices in 2016 and 2018 demonstrated typical characteristics, where the highest heat wave indices appeared over the northwestern and southeastern regions; the patterns correspond to typical heat wave patterns of South Korea (Yoon et al. 2018; K. H. Min et al. 2020). As TMAX patterns during heat wave events could be induced by an anticyclone covering South Korea entirely (Yoon et al.

2018), we analyzed the synoptic conditions by compositing for heat waves of 2016 and 2018.

Figure 5 describes a composite of the 500-hPa geopotential height anomaly for the 2016 and 2018 heat wave events from ERAIN data. A geopotential height anomaly was calculated by subtracting 39-yr climatological mean fields, during 1980–2018. Positive geopotential height anomalies exist for several heat wave events (e.g., 2016C, 2016D, and 2016E) over the Korean Peninsula. This prominent anomaly (anticyclone) over the Korean Peninsula could have primarily caused exceptional heat waves and typical spatial patterns of heat wave indices in the summers of 2016 and 2018 (Fig. 4). However, synoptic characteristics of height patterns between 2016 and 2018 vary. The centers of the geopotential heights for the 2016 heat wave events are located in northern China and Mongolia (Fig. 5). This position of the high pressure system could have induced warm advection by northerly winds blown from anomalously
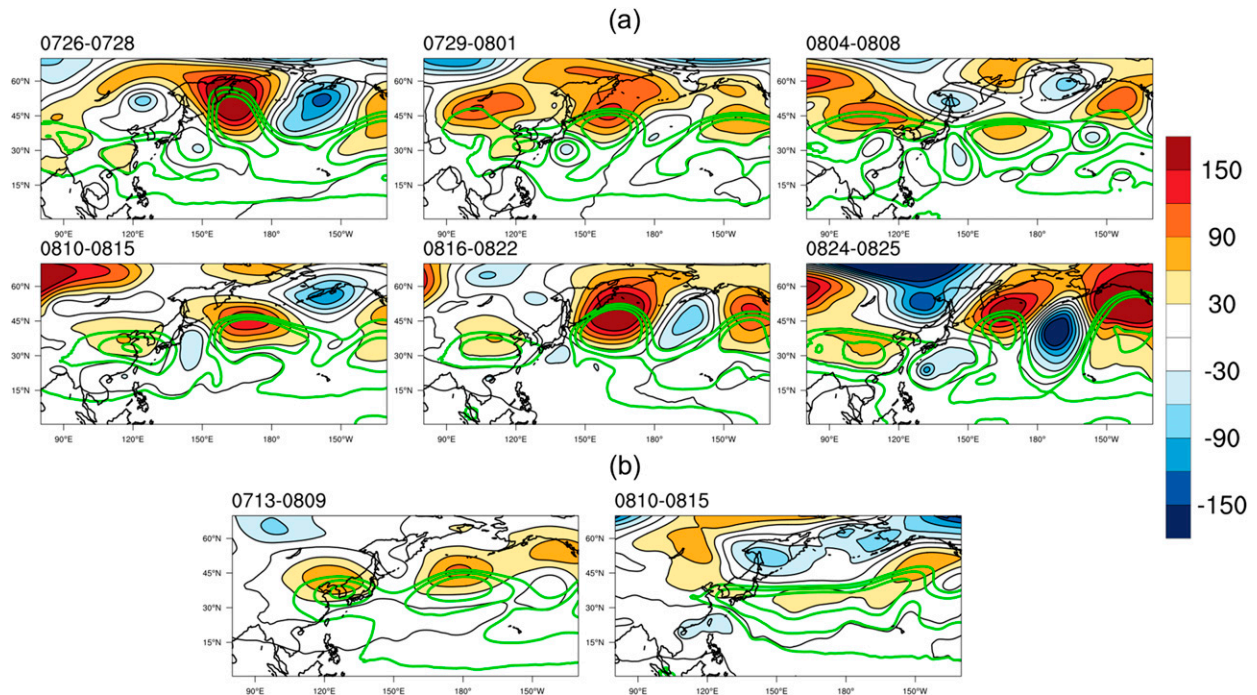
FIG. 5. The 500-hPa geopotential height anomaly (gpm) of the heat waves of (a) 2016 and (b) 2018. The green contour lines indicate geopotential heights of 5860, 5880, and 5900 gpm, respectively.

warm and dry regions (i.e., Mongolia and western Eurasia) in the 2016 summer (Yeh et al. 2018). Thus, an intense HWI in 2016D could have been caused by exceptional positive anomalies of geopotential heights over northern China and Mongolia. Other huge positive anomalies of geopotential heights over the Kamchatka Peninsula for the 2016 heat wave events exist; for example, in 2016E, there is a prominent blocking high over the Kamchatka Peninsula with a large expansion of the continental thermal high. According to the previous studies, the anomalous anticyclone over the Kamchatka Peninsula during a heat wave acts as atmospheric blocking, downstream of the Korean Peninsula, blocking the eastward movement of positive geopotential height anomalies over East Asia, causing long-lasting high-temperature events (Yeh et al. 2018; K. H. Min et al. 2020). As East Asia is one of the regions affected by prevailing westerlies, there exists an eastward mean flow in the midlevel atmosphere. When the anticyclone exists in the Kamchatka area, the zonal flow is blocked and the continental thermal high over the Korean Peninsula can be stagnant. As a large blocking high existed over the Kamchatka Peninsula during 2016E but the continental thermal high was slightly shrunken toward the west, it was seemingly not as prominent as that of 2016D (Fig. 4), but it lasted unusually longer, as previously noted. Conversely, the heat wave events of 2018 had a more typical synoptic pattern, as suggested by previous studies. A large expansion of the WNPSH existed during 2018A and 2018B (green contour lines in Fig. 5); this could have caused a heat wave over the Korean Peninsula by blowing warm low-level southerly winds along the WNPSH (Lee and Lee 2016; Yoon et al. 2018; Xu et al.

2019). In addition, a strong positive anomaly existed between the Kamchatka Peninsula and the Aleutian Islands during 2018A. Various studies have suggested that this zonally extended pattern of the geopotential height from the Korean Peninsula to the Aleutian Islands is as a typical feature of large-scale circulation in South Korea associated with a circumglobal teleconnection pattern in boreal summer (Ding et al. 2010; Lee and Lee 2016; Deng et al. 2019; M.-K. Kim et al. 2019; Kornhuber et al. 2019; Yeo et al. 2019; Choi et al. 2020). Briefly, typical spatial patterns of heat wave indices in the northwestern and southeastern regions of South Korea existed, as prominent anticyclones covered South Korea during the 2016 and 2018 heat wave events. However, the Kamchatka blocking and the continental high prevailed during the 2016 heat waves, while an expansion of the WNPSH and large-scale teleconnection were associated with the 2018 heat waves, respectively.

b. Numerical experiments

Simulations of the 2016 and 2018 heat wave events using the WRF Model were analyzed. Particularly, simulations of the blocking high over the Kamchatka Peninsula, which is one of the most representative characteristics of the heat waves in 2016, were evaluated in the NOSN experiment. Figure 6 describes the monthly mean 500-hPa geopotential height of the FNL and WRF Model results for July and August (JA) of 2016 and 2018. As described earlier, a prominent blocking high, clearly represented by an omega-shaped ridge (Rex 1950), existed over the Kamchatka region in August 2016; there was a large expansion of the WNPSH along the Korean Peninsula in
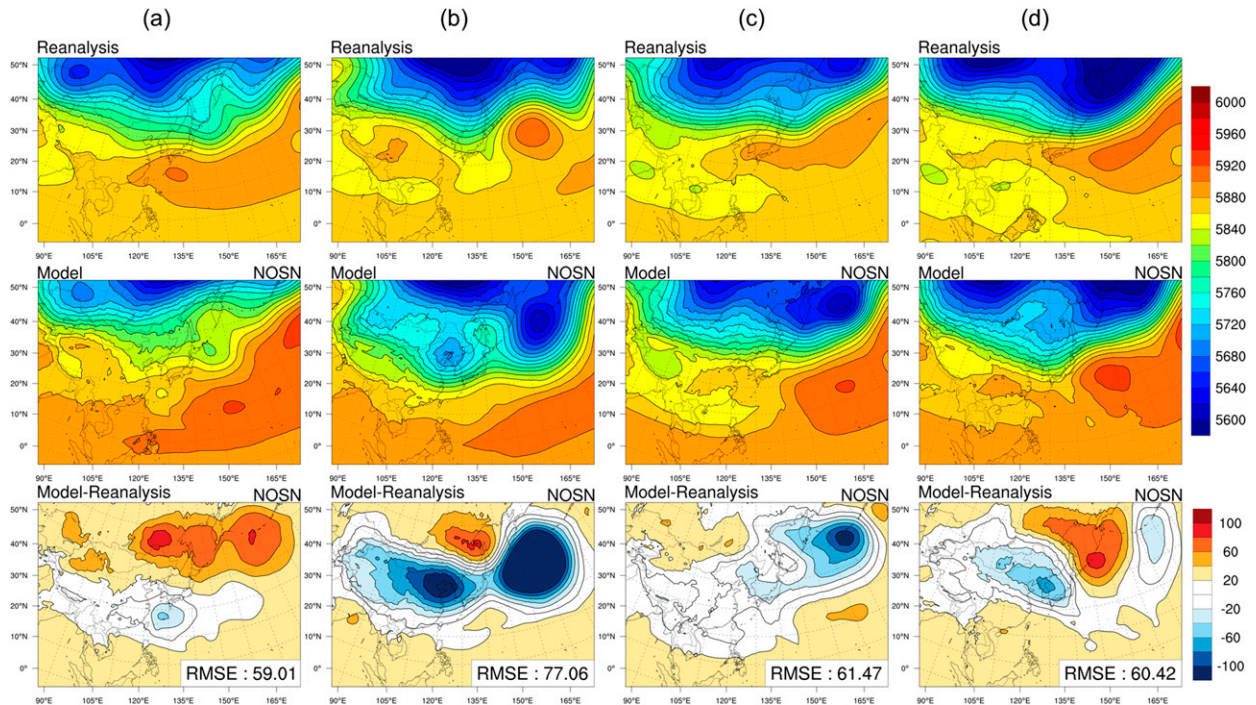
FIG. 6. Monthly mean 500-hPa geopotential height (gpm) in (top) the FNL data, (middle) the NOSN experiment, and (bottom) their differences over domain 1 during (a) July 2016, (b) August 2016, (c) July 2018, and (d) August 2018. The numbers in the bottom-right boxes indicate the area averages of RMSE over the entire domain 1, except for the buffer zone during each period.

JA 2018. These anomalous synoptic characteristics of heat waves need to be well simulated in a numerical model to produce a reasonable TMAX distribution. However, the simulation of the blocking for August 2016 (Fig. 6b) is unrealistic in comparison with other periods (i.e., July 2016 and JA 2018; Figs. 6a,c,d). In particular, the WRF Model simulates a trough rather than an omega-shaped ridge over the Kamchatka region. On comparing the WRF results and the FNL data, prominent negative biases of the midlevel geopotential height over the Kamchatka Peninsula as well as the Korean Peninsula during August 2016 exist. Quantitatively, the root-mean-square error (RMSE) of the geopotential height over domain 1 entirely, except for the buffer zone, increased from 59.01 to 77.06 in July and August 2016, respectively; while those for July and August 2018 were 61.47 and 60.42, respectively, lower than that of August 2016. Despite some biases in geopotential height, the overall atmospheric systems were reasonably simulated for July 2016 and JA 2018, whereas that of August 2016 had a different structure, notably over the Kamchatka Peninsula and the Korean Peninsula.

As the Kamchatka blocking and the continental thermal high over Mongolia were underestimated in the WRF Model for August 2016, temporal changes of anticyclones over both areas were analyzed using the Hovmöller plot (Fig. 7). Three high peaks of the 500-hPa geopotential height over the Kamchatka area (40°–60°N, 145°E–180°) during JA 2016 exist (Fig. 7a). Particularly, the second and third peaks of the geopotential height in late July and mid–late August 2016 play a role of the blocking high; this period coincides with the heat waves over South Korea

in 2016. Moreover, the expansion of the thermal high in the Korean Peninsula area (25–45°N, 115–140°E) begins from 20 July, becoming most extreme in mid-August (Fig. 7b); as analyzed previously, this feature is distinguishable with the expansion of the WNPSH during summer 2018. The heat waves of 2016 were seemingly induced by the development of the third blocking event with a continental thermal high during the same period. Conversely, in the WRF simulation, the last peak of the blocking high that starts from mid-August disappears; the model significantly underestimates the geopotential height during July and August 2016. Thus, a continental thermal high is unable to prevail and develop due to the absence of the Kamchatka blocking, which prevents the midlatitude atmospheric system from moving eastward. Therefore, strong negative biases exist over both regions, occurring at the same time. This implies that typical features of the 2016 heat wave were not well captured by the WRF Model, although the simulation for JA 2018 demonstrated a relatively reasonable feature; this limitation could cause significant errors in surface air temperature for the 2016 heat wave.

Conversely, the blocking high over the Kamchatka Peninsula during 2016 is well reproduced in the SN experiment. In Fig. 8, the blocking ridge, which was not reproduced in the NOSN experiment, was well simulated over the Kamchatka Peninsula for August 2016. Consequently, the geopotential height difference between the FNL and simulated result significantly decreased over the region due to the effect of SN. Despite decreased biases for JA 2018, the RMSE over the entire domain improved the most for August 2016, quantitatively. The simulation of the continental thermal high, extending over the
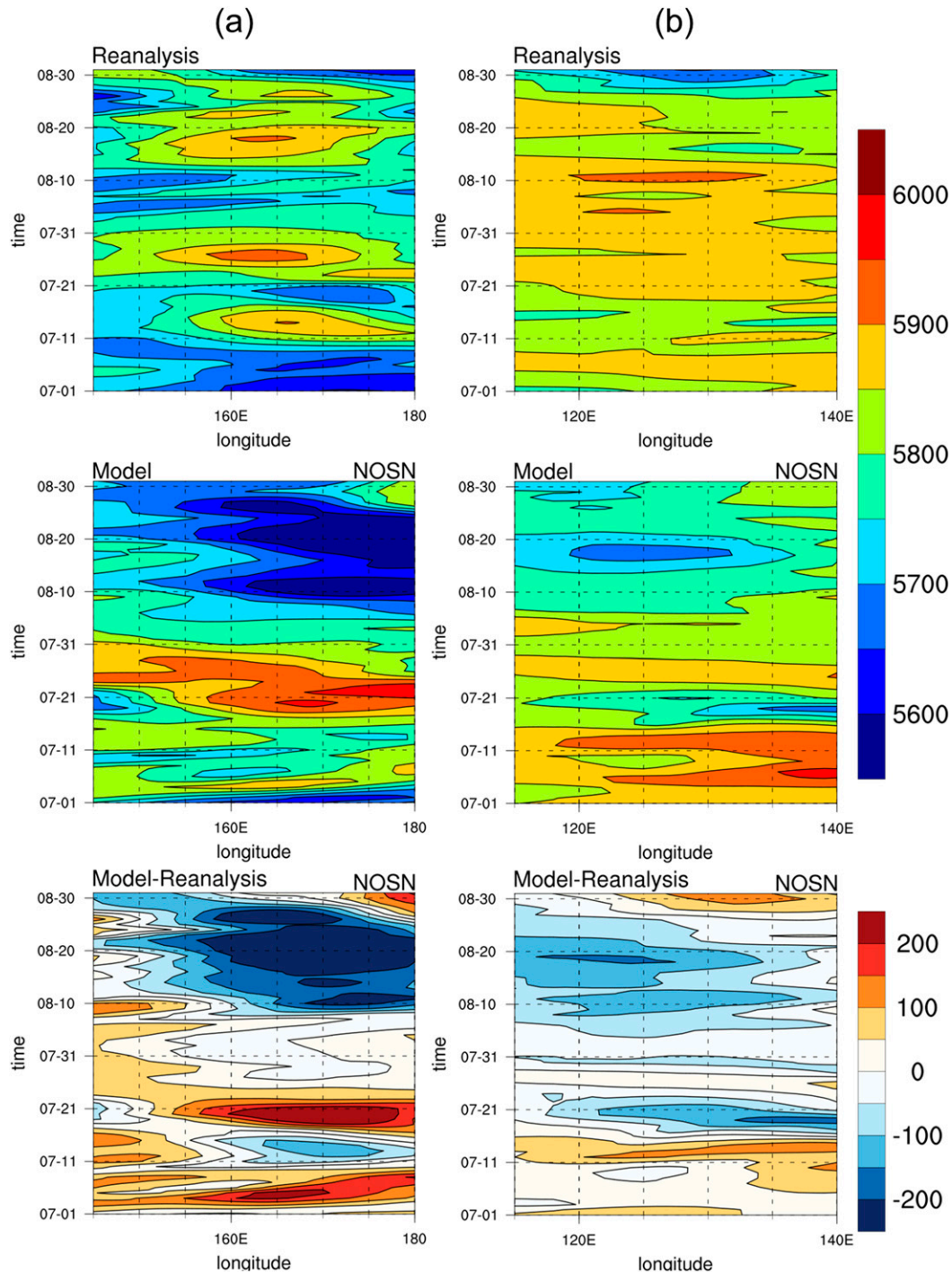
FIG. 7. Hovmöller plot of the 500-hPa geopotential height (gpm) in (top) the FNL data, (middle) the NOSN experiment, and (bottom) their differences over (a) the Kamchatka area (40°–60°N, 145°E–180°) and (b) the Korean Peninsula (25°–45°N, 115°–140°E) during JA 2016.

Korean Peninsula, was somewhat improved in the SN experiment, but a negative bias prevailed for August 2016. This suggests that not only blocking over the Kamchatka Peninsula but also other synoptic factors such as the continental thermal

high could be essential in improving the simulation of the 2016 heat wave.

Figure 9 shows the Hovmöller plot over the Kamchatka Peninsula and the Korean Peninsula for JA 2016 in the SN
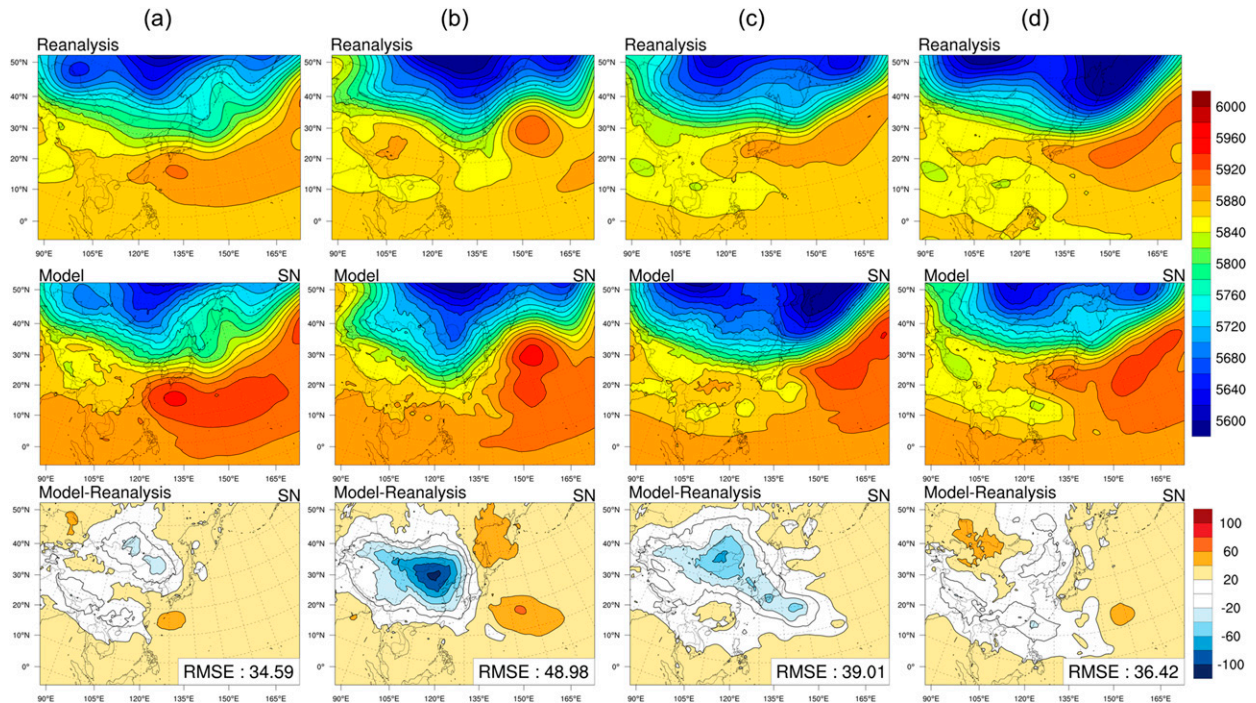
FIG. 8. Monthly mean 500-hPa geopotential height (gpm) in (top) the FNL data, (middle) the SN experiment, and (bottom) their differences over domain 1 during (a) July 2016, (b) August 2016, (c) July 2018, and (d) August 2018. The numbers in the bottom-right boxes indicate the area averages of RMSE over the entire domain 1, except for the buffer zone during each period.

experiment. The three peaks of the blocking high over the Kamchatka region are realistically captured, and the pattern of geopotential height in the SN experiment coincides with the reanalysis data; in particular, the third peak of the geopotential height during mid-August 2016, which was not reproduced in the NOSN experiment, is reasonably simulated. Around the Korean Peninsula, the geopotential height bias is also notably reduced in the SN experiment, although SN was only applied over the Kamchatka area; in particular, a negative bias of geopotential height appearing 15 August onward was decreased. However, a limitation of the model persists; the expansion of the continental thermal high was underestimated during 4–15 August, which is one of the factors that caused the most severe heat wave in 2016 (i.e., 2016D). Contrarily, the negative bias of geopotential height over the Korean Peninsula in 2016E, when the blocking high was strongest, is insignificant.

Daily RMSEs of 500-hPa geopotential height averaged over the Kamchatka area and other regions during JA 2016 are represented in Fig. 10. The area-averaged RMSE over the Kamchatka area of the SN experiment was relatively small, having no significant variation for the analysis period, while that of the NOSN experiment exceeded 100 gpm, being highest in mid-August when the Kamchatka blocking was the most intense, for example, the maximum RMSE averaged over the Kamchatka area in the NOSN experiment reached about 300 gpm for 20 August, whereas it was about 55 gpm in the SN experiment. Conversely, the averaged RMSEs over the entire model domain, except for the Kamchatka area, demonstrated a relatively small difference between the NOSN and SN

experiments. The WRF Model somewhat understated 500-hPa geopotential height during the July–August period of 2018, but quantitatively, it had better-simulated performance compared to those of August 2016. RMSEs that averaged in the Kamchatka region during the heat wave events were 167 gpm in 2016 and 116 gpm in 2018. In addition, the RMSE exceeded nearly 300 gpm in 2016 when blocking was strongest, but there was no significant variability in 2018 during the analysis period (not shown). Thus, the WRF Model without SN was unable to simulate blocking over the Kamchatka Peninsula, which was a significant factor of the extreme heat wave in mid-August 2016; the Kamchatka blocking was reasonably reproduced in the SN experiment through the SN technique.

To evaluate the effects of synoptic conditions on the heat wave events in South Korea, spatial distributions of TMAX between the WRF simulation and ASOS observation were compared (Fig. 11). As the simulated TMAX for domain 1 was relatively coarse when compared to the observed data, the modeling result of the higher-resolution case (domain 2) was also analyzed. Thus, TMAX biases caused by lower resolution could be improved in the result of domain 2. In general, TMAX over South Korea in 2016 and 2018 was underestimated across all experiments. These cold biases of TMAX over South Korea could be interpreted as a systematic error of the WRF Model, pointed out by Im et al. (2015). The negative biases were more significant in the southeastern than the northwestern region of South Korea in two years, despite the severe heat waves in both regions as discussed earlier. The difference in TMAX biases between both regions during the heat wave events could be
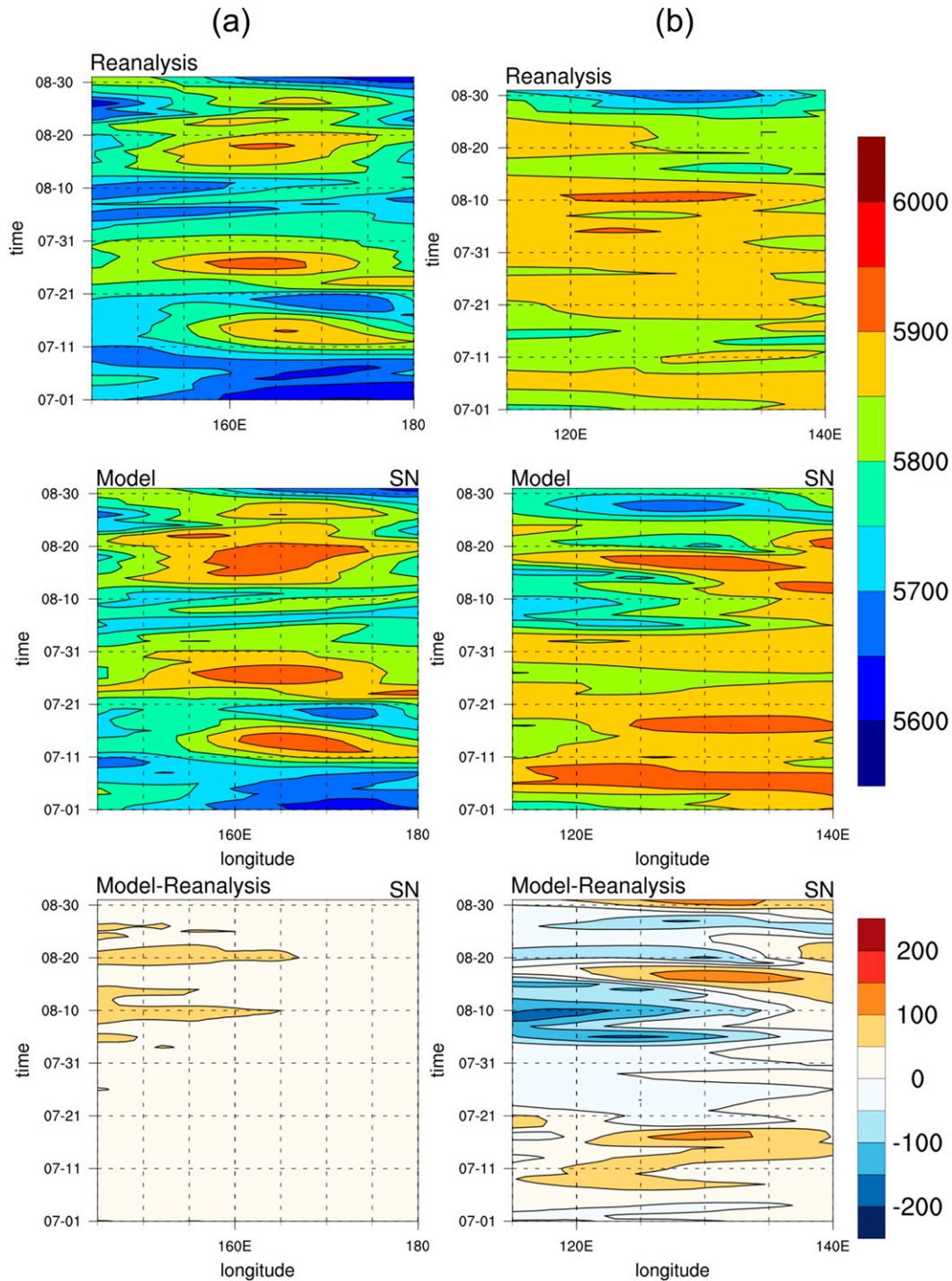
FIG. 9. Hovmöller plot of the 500-hPa geopotential height (gpm) in (top) the FNL data, (middle) the SN experiment, and (bottom) their differences over (a) the Kamchatka area (40–60 °N, 145°E–180°) and (b) the Korean Peninsula (25°–45°N, 115°–140°E) during JA 2016.

caused by the relatively complex topography over the southeastern region of South Korea (Yoon et al. 2018). As the simulation of the anomalous synoptic geopotential height patterns affecting the heat wave events over South Korea was

worse for 2016 than for 2018, the TMAX errors were greater for 2016 and the intensity of heat wave events was more severe in 2018. Considering the NOSN experiments, the averaged RMSE of TMAX in 2016 over South Korea was ~0.8°C higher
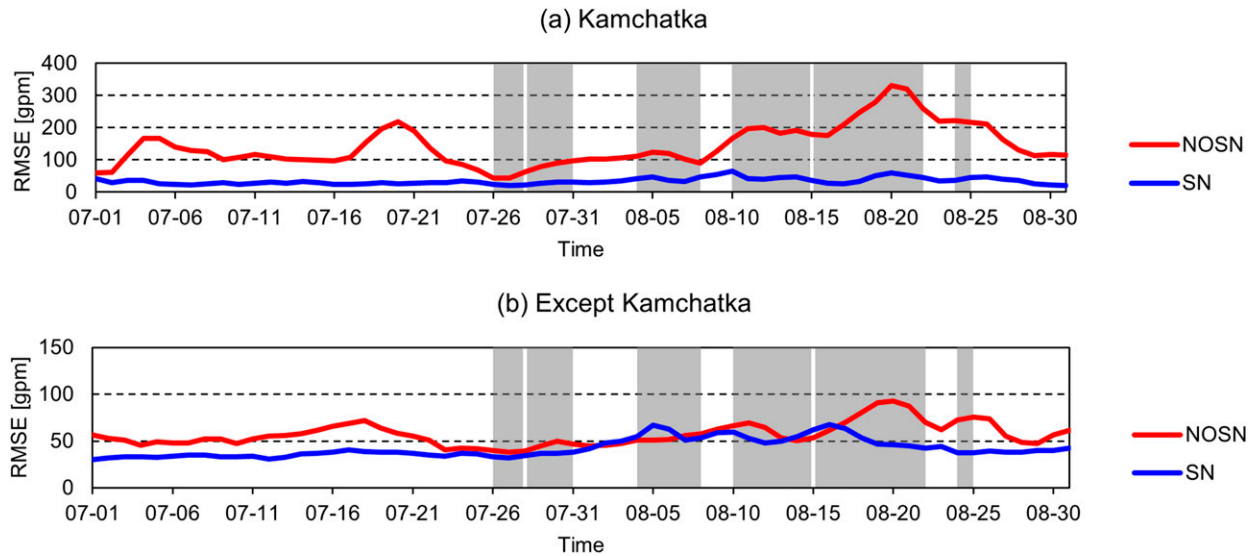
(a) Kamchatka

(b) Except Kamchatka

FIG. 10. Time series of daily RMSE of the 500-hPa geopotential height (gpm) over (a) the Kamchatka Peninsula area (40°–60°N, 145°E–180°) and (b) domain 1, except the Kamchatka Peninsula area in the NOSN (red) and the SN (blue) experiments during JA 2016. The gray shaded boxes indicate the heat waves.

than that of 2018 in domains 1 and 2. This TMAX bias was reduced by applying SN over the Kamchatka area. The reduction of RMSE in the SN experiment was considerably greater for 2016 than for 2018; particularly, the RMSE of domain 2 decreased by 0.7°C in 2016 while there was no significant change in 2018. Figure 12 represents temporal changes of TMAX RMSE over South Korea in domains 1 and 2 during JA 2016. For most of the analysis period, the TMAX

RMSEs of the NOSN experiment in both resolutions decreased on the application of SN. In particular, in both domains, the TMAX RMSEs of the NOSN experiment were substantially reduced for 2016E, in which the intensity of the blocking high was the most robust. It indicates that the WRF Model could capture the unusually long duration of the 2016E heat wave if the blocking high were reproduced realistically. In other words, this demonstrates that
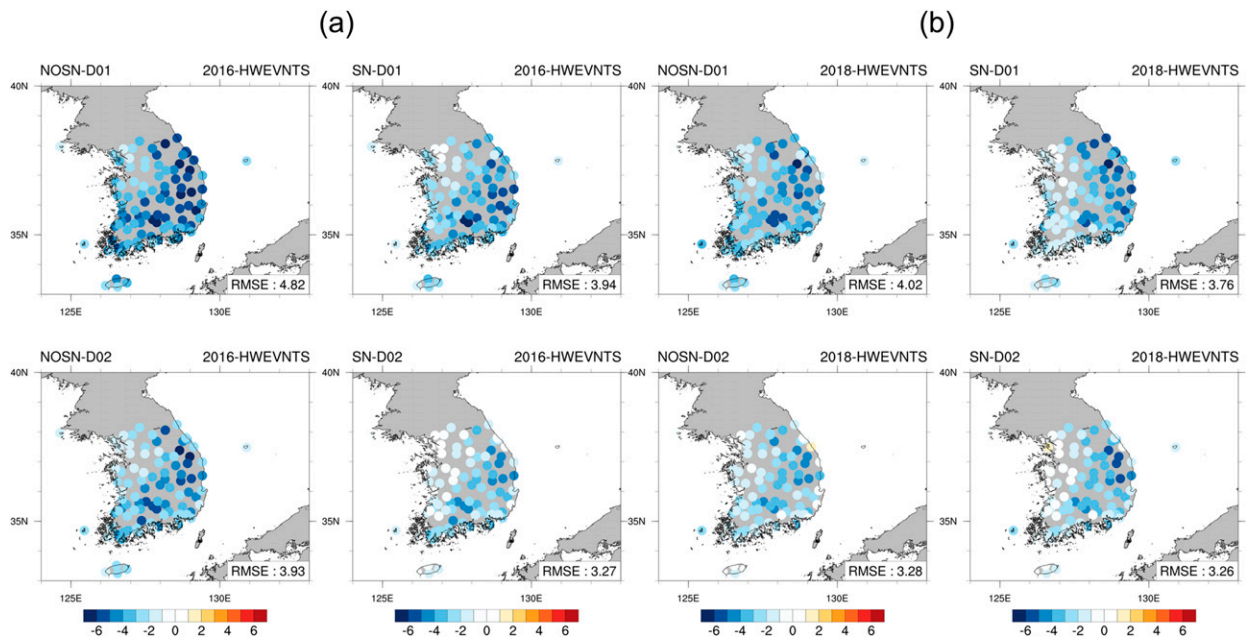

FIG. 11. Spatial distributions of TMAX bias (°C) between the WRF and ASOS stations for (top) domain 1 and (bottom) domain 2 in (left) the NOSN and (right) the SN experiments during the (a) 2016 and (b) 2018 heat waves.
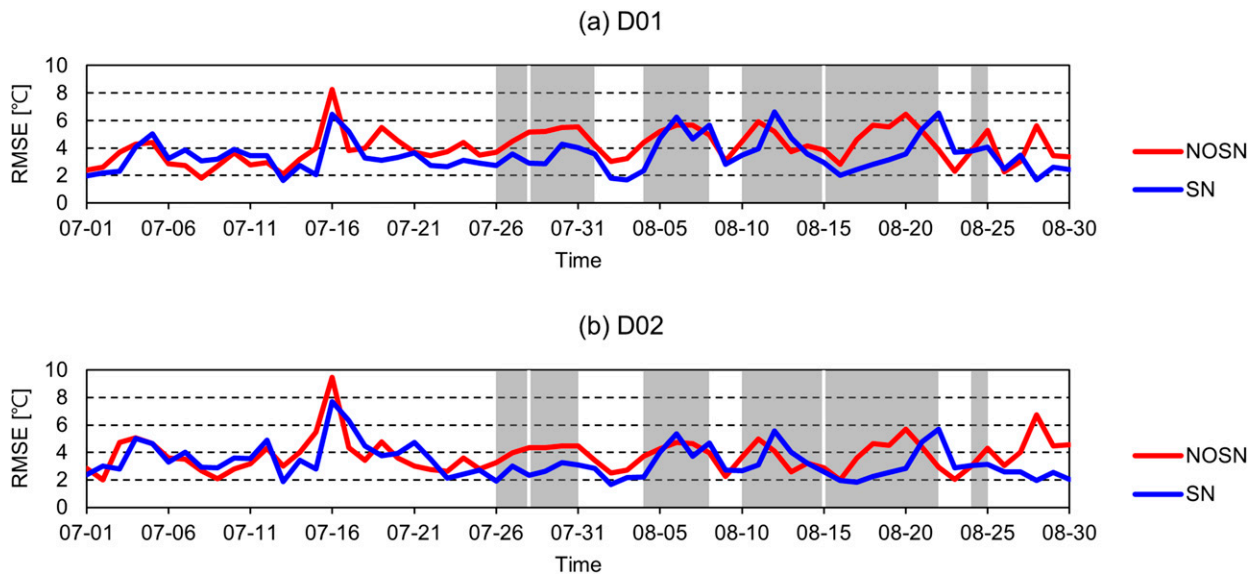
FIG. 12. Time series of TMAX RMSE (°C) between the WRF and ASOS stations for (a) domain 1 and (b) domain 2 in the NOSN and the SN experiments during 2016 JA. The gray shaded boxes indicate the heat waves.

the Kamchatka blocking mainly contributed to the 2016E heat wave. Unlike in 2016E, the TMAX RMSEs during 2016D showed no significant difference between the NOSN and the SN experiments for domains 1 and 2, even though this period was the most extreme in terms of heat waves in South Korea. It could be associated with the unresolved bias of geopotential height over northern China in the SN experiment, as described in Fig. 9.

4. Summary and discussion

In this study, the meteorological characteristics of the 2016 and 2018 heat wave events over South Korea were first analyzed. The annual accumulated HWD of the 2016 and 2018 heat wave events, which was defined using spatiotemporal criteria, was recorded as the third and first longest, respectively, over 39 years (1980–2018). In terms of indices representing the intensity of heat wave events, the events of 2016 and 2018 also highly ranked among 97 heat wave events; the events of 2016D, 2018A, and 2018B, in particular, were the most extreme. Synoptic characteristics of the extreme heat wave events in 2016 and 2018 were analyzed to examine their causes; this demonstrated a significant positive anomaly of the 500-hPa geopotential height, which could have induced warm conditions over the Korean Peninsula in both years. However, we observed a blocking high over the Kamchatka Peninsula and a continental thermal high from northern China and Mongolia during the 2016 heat wave events, while an expansion of the WNPSH was associated with the 2018 heat wave events. Subsequently, numerical experiments using the WRF Model were conducted to assess if these synoptic features were adequately reproduced in the RCM; we analyzed the effect of these synoptic conditions on the studied heat wave events. Consequently, the blocking high during

mid–late August 2016 was underestimated in the NOSN experiment, while the large expansion of the WNPSH along the Korean Peninsula in JA 2018 was reasonably represented. Thus, the continental thermal high was unable to stagnate and develop due to the absence of the Kamchatka blocking until late August 2016. The blocking high of 2016 was realistically reproduced in the SN experiment, and the geopotential height bias over the Korean Peninsula in 2016E was reduced, even though nudging was only applied over the Kamchatka region. In terms of TMAX, the negative biases were more significant for the summer of 2016 than 2018, although the intensity of heat waves was more severe in 2018. TMAX RMSE was substantially reduced for 2016E, in which the influence of the blocking high was the strongest. Hence, the anticyclone over Kamchatka, which was a distinctive synoptic feature of the 2016 heat wave, was not well simulated by the WRF Model, which simulated an early end of the 2016 heat wave over the Korean Peninsula. Consequently, this study is meaningful in that 1) the response of the South Korea heat wave in 2016 by the existence of Kamchatka blocking was investigated, and 2) the necessity of improving simulation performance for the Kamchatka blocking in the RCM during heat wave was suggested.

The WRF Model failed to simulate the distinct synoptic characteristics of heat wave events in 2016, implying that challenges could exist in simulating the intensity or duration of a 2016-type heat wave in an RCM. Several studies revealed that the frequency of summer blocking in the Okhotsk region has been increasing over recent decades, using observational data and ensemble climate models (Li et al. 2017; Lupo et al. 2019; Mokhov and Timazhev 2019; Yoon et al. 2020). Moreover, Meng et al. (2020) reported that extreme temperature events in China's Inner Mongolia have been increasing under representative concentration pathway scenarios.
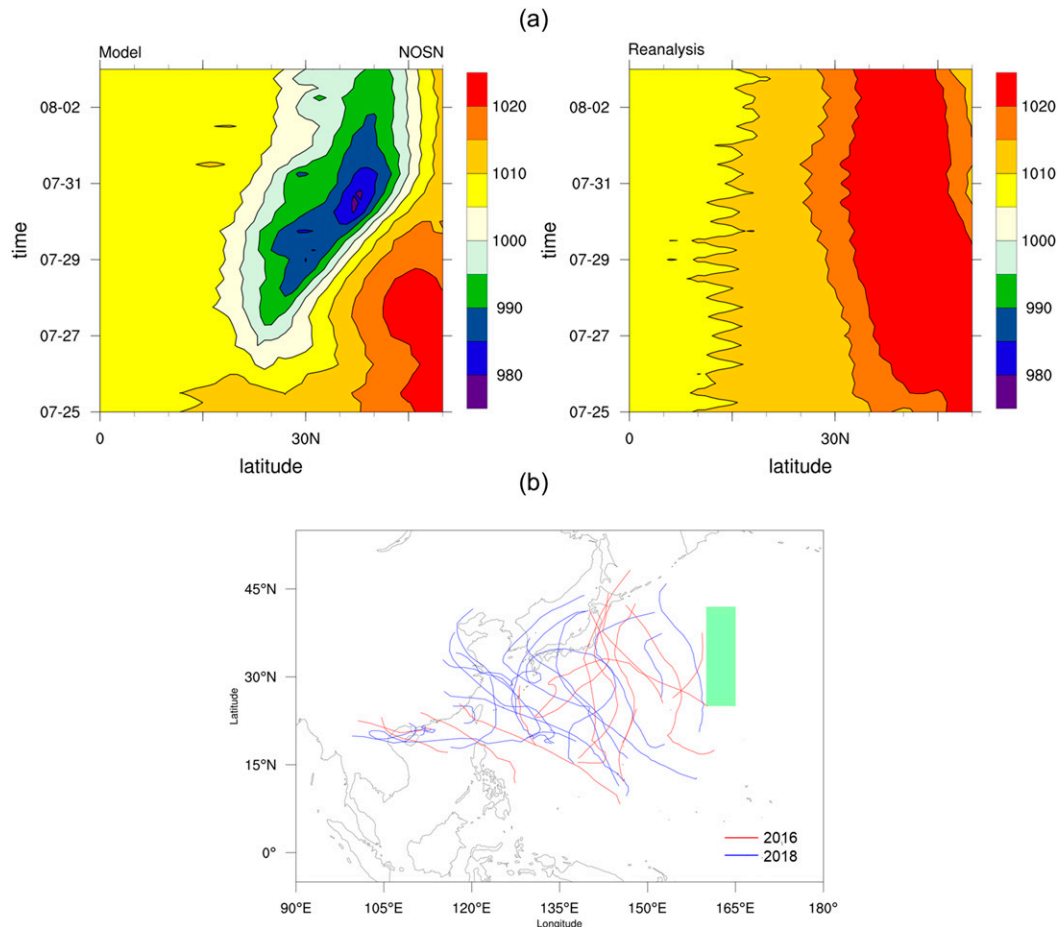
FIG. 13. (a) Hovmöller plot of sea level pressure (hPa) over the North Pacific region (0°–50°N, 160°–165°E) during 25 Jul–3 Aug 2016 in (left) the NOSN experiment and (right) the ERAIN data. (b) Best tracks of typhoons during JA 2016 and 2018. The green shaded box indicates the North Pacific region.

Therefore, it is necessary to improve the simulation of the blocking and continental thermal high over East Asia.

Various atmospheric factors could influence the simulation of the summer blocking high in an RCM. In particular, reproducing tropical cyclones realistically over the western North Pacific in a numerical model is key to predicting summer weather in the midlatitudes, as the extratropical transition of tropical cyclones can significantly influence the evolution of the midlatitude blocking downstream; such structural changes often contribute to significant errors in numerical forecasts (Evans et al. 2006; Harr et al. 2008; Riboldi et al. 2019). In addition, uncertainties exist in simulating the genesis and activities of tropical cyclones over the western North Pacific using RCMs (Cha et al. 2011b; Jin et al. 2016). Jin et al. (2016) evaluated tropical cyclone activity over the western North Pacific using five different RCMs driven by ERAIN data for the period 1989–2008. They demonstrated that even if the WRF has the most realistic spatial patterns of tropical cyclone genesis frequency as compared to the other models, biases of the genesis frequency will persist. Here, the WRF Model simulated spurious tropical cyclones that did not exist

in summer 2016, and one of them perturbed midlatitude wave by the transition to an extratropical cyclone. Figure 13a represents the temporal evolution of sea level pressure over the North Pacific region (0°–50°N, 160°–165°E) during late July 2016 in the NOSN experiment and the reanalysis data. The WRF Model without SN demonstrated an unrealistic simulation of the development of a low pressure system from late July to early August 2016, while a high pressure system was dominant for the period in the reanalysis data. This unrealistic cyclone in the NOSN experiment interacted with the midlatitude wave and obstructed the formation of a blocking ridge, represented in the reanalysis data. Based on the official best track data from the Joint Typhoon Warning Center, the typhoon tracks in JA 2016 were generally lopsided, more northeastwardly, than those in JA 2018 (Fig. 13b); for instance, no typhoon approached the Korean Peninsula and East China in JA 2016. This is seemingly due to the weak expansion of the WNPSH in 2016, inducing a more poleward movement of typhoons (Ho et al. 2004; Lee et al. 2019). Hence, there could have been more chances for the tropical cyclone to extratropical transition and interact with the

blocking ridge in the Kamchatka area. Consequently, the simulation error of tropical cyclones in the RCM could also fail to simulate heat waves associated with the Kamchatka blocking. Hence, the RCM needs to improve its simulation of the physical processes of the convective system, such as tropical cyclones, and reproduce a detailed air–sea interaction process over the western North Pacific using a coupled model to simulate the summer weather system more reasonably.

The simulation of TMAX during 2016E was significantly associated with the simulation of the Kamchatka blocking. However, as represented in Figs. 9 and 12, the WRF Model could not capture the expansion of the continental thermal high during 2016D; the TMAX error during 2016D demonstrated no significant difference between the NOSN and the SN experiments, even if this period were the most extreme heat wave event in South Korea. These results suggest that not only blocking over Kamchatka but also the development of an anticyclone over northern China in the WRF Model could affect the TMAX error during this period. According to previous studies, an anticyclone and dry land surface state could be related to each other during a heat wave (Erdenebat and Sato 2016; Sato and Nakamura 2019; Seo et al. 2020; Zhang et al. 2020); hence, initial soil moisture conditions over the area in a numerical model could affect the heat wave simulation (Fischer et al. 2007; Yoon et al. 2018; Seo et al. 2019). Seo et al. (2019) demonstrated that the prediction of boreal summer surface air temperature could be improved using data on the initial soil moisture conditions, taken from an observation-driven offline land surface model simulation. Thus, accurate data on initial soil moisture conditions are needed to improve numerical weather prediction during heat waves like that of summer 2016.

The ensemble mean is one of the effective ways to improve the prediction performance of numerical models. KMA has a local ensemble prediction system (LENS) and ensemble prediction system (EPS) for the short-term and medium-range forecasting of heat wave events. Although ensemble forecasting systems can improve the prediction skill of the representative synoptic conditions of heat wave event (Matsueda 2011), the 2016 heat wave lasted longer than KMA expected, as high temperatures were underestimated in the medium-range forecast system. Therefore, the improvement of the blocking prediction in the ensemble forecasting system is needed. Since all the experiments integrated only once, this study did not highlight the methods for improving predictability in terms of the ensemble mean. Further studies related to the ensemble mean are required to improve the predictability of 2016-type heat wave events.

REFERENCES

Barnes, S. L., 1964: A technique for maximizing details in numerical weather map analysis. *J. Appl. Meteor.*, **3**, 396–409, https://doi.org/10.1175/1520-0450(1964)003<0396:ATFMDI>2.0.CO;2.

Barriopedro, D., E. M. Fischer, J. Luterbacher, R. M. Trigo, and R. García-Herrera, 2011: The hot summer of 2010: Redrawing the temperature record map of Europe. *Science*, **332**, 220–224, https://doi.org/10.1126/science.1201224.

Black, E., M. Blackburn, G. Harrison, B. Hoskins, and J. Methven, 2004: Factors contributing to the summer 2003 European heatwave. *Weather*, **59**, 217–223, https://doi.org/10.1256/wea.74.04.

Bowden, J. H., T. L. Otte, C. G. Nolte, and M. J. Otte, 2012: Examining interior grid nudging techniques using two-way nesting in the WRF Model for regional climate modeling. *J. Climate*, **25**, 2805–2823, https://doi.org/10.1175/JCLI-D-11-00167.1.

Cha, D.-H., and D.-K. Lee, 2009: Reduction of systematic errors in regional climate simulations of the summer monsoon over East Asia and the western North Pacific by applying the spectral nudging technique. *J. Geophys. Res.*, **114**, D14108, https://doi.org/10.1029/2008JD011176.

——, C.-S. Jin, and D.-K. Lee, 2011a: Impact of local sea surface temperature anomaly over the western North Pacific on extreme East Asian summer monsoon. *Climate Dyn.*, **37**, 1691–1705, https://doi.org/10.1007/s00382-010-0983-z.

——, ——, ——, and Y.-H. Kuo, 2011b: Impact of intermittent spectral nudging on regional climate simulation using Weather Research and Forecasting model. *J. Geophys. Res.*, **116**, D10103, https://doi.org/10.1029/2010JD015069.

——, and Coauthors, 2016: Future changes in summer precipitation in regional climate simulations over the Korean Peninsula forced by multi-RCP scenarios of HadGEM2-AO. *Asia-Pac. J. Atmos. Sci.*, **52**, 139–149, https://doi.org/10.1007/s13143-016-0015-y.

Choi, N., and M.-I. Lee, 2019: Spatial variability and long-term trend in the occurrence frequency of heatwave and tropical night in Korea. *Asia-Pac. J. Atmos. Sci.*, **55**, 101–114, https://doi.org/10.1007/s13143-018-00101-w.

——, ——, D.-H. Cha, Y.-K. Lim, and K.-M. Kim 2020: Decadal changes in the interannual variability of heatwaves in East Asia caused by atmospheric teleconnection changes. *J. Climate*, **33**, 1505–1522, https://doi.org/10.1175/JCLI-D-19-0222.1.

Coumou, D., A. Robinson, and S. Rahmstorf, 2013: Global increase in record-breaking monthly-mean temperatures. *Climatic Change*, **118**, 771–782, https://doi.org/10.1007/s10584-012-0668-1.

Dee, D. P., and Coauthors, 2011: The ERA-Interim reanalysis: Configuration and performance of the data assimilation system. *Quart. J. Roy. Meteor. Soc.*, **137**, 553–597, https://doi.org/10.1002/qj.828.

Deng, K, S. Yang, A. Lin, C. Li, and C. Hu, 2019: Unprecedented East Asian warming in spring 2018 linked to the North Atlantic tripole SST mode. *Atmos. Ocean. Sci. Lett.*, **12**, 246–253, https://doi.org/10.1080/16742834.2019.1605807.

Ding, T., W. Qian, and Z. Yan, 2010: Changes in hot days and heat waves in China during 1961–2007. *Int. J. Climatol.*, **30**, 1452–1462, https://doi.org/10.1002/joc.1989.

Erdenebat, E., and T. Sato, 2016: Recent increase in heat wave frequency around Mongolia: Role of atmospheric forcing and possible influence of soil moisture deficit. *Atmos. Sci. Lett.*, **17**, 135–140, https://doi.org/10.1002/asl.616.

Evans, J. L., J. M. Arnott, and F. Chiaromonte, 2006: Evaluation of operational model cyclone structure forecasts during extratropical transition. *Mon. Wea. Rev.*, **134**, 3054–3072, https://doi.org/10.1175/MWR3236.1.

Fischer, E. M., S. I. Seneviratne, P. L. Vidale, D. Lüthi, and C. Schär, 2007: Soil moisture–atmosphere interactions during the 2003 European summer heat wave. *J. Climate*, **20**, 5081–5099, https://doi.org/10.1175/JCLI4288.1.

Giorgi, F., and M. R. Marinucci, 1996: A investigation of the sensitivity of simulated precipitation to model resolution and its implications for climate studies. *Mon. Wea. Rev.*, **124**, 148–166, https://doi.org/10.1175/1520-0493(1996)124<0148:AIOTSO>2.0.CO;2.

Harr, P. A., D. Anwender, and S. C. Jones, 2008: Predictability associated with the downstream impacts of the extratropical transition of tropical cyclones: Methodology and a case study of Typhoon Nabi (2005). *Mon. Wea. Rev.*, **136**, 3205–3225, https://doi.org/10.1175/2008MWR2248.1.

Harris, L. M., and D. R. Durran, 2010: An idealized comparison of one-way and two-way grid nesting. *Mon. Wea. Rev.*, **138**, 2174–2187, https://doi.org/10.1175/2010MWR3080.1.

Ho, C. H., J. J. Baik, J. H. Kim, D. Y. Gong, and C. H. Sui, 2004: Interdecadal changes in summertime typhoon tracks. *J. Climate*, **17**, 1767–1776, https://doi.org/10.1175/1520-0442(2004)017<1767:ICISTT>2.0.CO;2.

Hong, S.-Y., and E. Kalnay, 2002: The 1998 Oklahoma–Texas drought: Mechanistic experiments with NCEP global and regional models. *J. Climate*, **15**, 945–963, https://doi.org/10.1175/1520-0442(2002)015<0945:TOTDME>2.0.CO;2.

——, and J.-O. J. Lim, 2006: The WRF single-moment 6-class microphysics scheme (WSM6). *J. Korean Meteor. Soc..*, **42**, 129–151.

——, Y. Noh, and J. Dudhia, 2006: A new vertical diffusion package with an explicit treatment of entrainment processes. *Mon. Wea. Rev.*, **134**, 2318–2341, https://doi.org/10.1175/MWR3199.1.

Iacono, M. J., J. S. Delamere, E. J. Mlawer, M. W. Shephard, S. A. Clough, and W. D. Collins, 2008: Radiative forcing by long-lived greenhouse gases: Calculations with the AER radiative transfer models. *J. Geophys. Res.*, **113**, D13103, https://doi.org/10.1029/2008JD009944.

Im, E.-S., J.-B. Ahn, and S.-R. Jo, 2015: Regional climate projection over South Korea simulated by the HadGEM2-AO and WRF model chain under RCP emission scenarios. *Climate Res.*, **63**, 249–266, https://doi.org/10.3354/cr01292.

——, N.-X. Thanh, Y.-H. Kim, and J.-B. Ahn, 2019: 2018 summer extreme temperatures in South Korea and their intensification under 3° C global warming. *Environ. Res. Lett.*, **14**, 094020, https://doi.org/10.1088/1748-9326/ab3b8f.

IPCC, 2013: *Climate Change 2013: The Physical Science Basis.* Cambridge University Press, 1535 pp., https://doi.org/10.1017/CBO9781107415324.

Jin, C.-S., D.-H. Cha, D.-K. Lee, M.-S. Suh, S.-Y. Hong, H.-S. Kang, and C.-H. Ho, 2016: Evaluation of climatological tropical cyclone activity over the western North Pacific in the CORDEX-East Asia multi-RCM simulations. *Climate Dyn.*, **47**, 765–778, https://doi.org/10.1007/s00382-015-2869-6.

Kain, J. S., 2004: The Kain–Fritsch convective parameterization: An update. *J. Appl. Meteor.*, **43**, 170–181, https://doi.org/10.1175/1520-0450(2004)043<0170:TKCPAU>2.0.CO;2.

Kim, D.-W., R. C. Deo, J.-H. Chung, and J.-S. Lee, 2015: Projection of heat wave mortality related to climate change in Korea. *Nat. Hazards*, **80**, 623–637, https://doi.org/10.1007/s11069-015-1987-0.

Kim, J., D. Yoon, D. H. Cha, Y. Choi, J. Kim, and S. W. Son, 2019: Impacts of the East Asian winter monsoon and local sea surface temperature on heavy snowfall over the Yeongdong region. *J. Climate*, **32**, 6783–6802, https://doi.org/10.1175/JCLI-D-18-0411.1.

Kim, M.-K., J.-S. Oh, C.-K. Park, S.-K. Min, K.-O. Boo, and J.-H. Kim, 2019: Possible impact of the diabatic heating over the Indian subcontinent on heat waves in South Korea. *Int. J. Climatol.*, **39**, 1166–1180, https://doi.org/10.1002/joc.5869.

Kornhuber, K., S. Osprey, D. Coumou, S. Petri, V. Petoukhov, S. Rahmstorf, and L. Gray, 2019: Extreme weather events in early summer 2018 connected by a recurrent hemispheric wave-7 pattern. *Environ. Res. Lett.*, **14**, 054002, https://doi.org/10.1088/1748-9326/ab13bf.

Kysely, J., and J. Kim, 2009: Mortality during heat waves in South Korea, 1991 to 2005: How exceptional was the 1994 heat wave? *Climate Res.*, **38**, 105–116, https://doi.org/10.3354/cr00775.

Larsen, J., 2003: Record heat wave in Europe takes 35,000 lives: Far greater losses may lie ahead. Plan B Updates, Earth Policy Institute, http://www.earth-policy.org/plan_b_updates/2003/update29.

Lee, H. D., K. H. Min, J. H. Bae, and D. H. Cha, 2020: Characteristics and comparison of 2016 and 2018 heat wave in Korea (in Korean). *Atmosphere*, **30**, 1–15, https://doi.org/10.14191/Atmos.2014.24.1.001.

Lee, M., D. H. Cha, J. Moon, J. Park, C. S. Jin, and J. C. Chan, 2019: Long-term trends in tropical cyclone tracks around Korea and Japan in late summer and early fall. *Atmos. Sci. Lett.*, **20**, e939, https://doi.org/10.1002/asl.939.

Lee, W.-S., and M.-I. Lee, 2016: Interannual variability of heat waves in South Korea and their connection with large-scale atmospheric circulation patterns. *Int. J. Climatol.*, **36**, 4815–4830, https://doi.org/10.1002/joc.4671.

Li, Y., P. Ye, Z. Pu, J. Feng, B. Ma, and J. Wang, 2017: Historical statistics and future changes in long-duration blocking highs in key regions of Eurasia. *Theor. Appl. Climatol.*, **130**, 1195–1207, https://doi.org/10.1007/s00704-017-2079-8.

Lupo, A. R., A. D. Jensen, I. I. Mokhov, A. V. Timazhev, T. Eichler, and B. Efe, 2019: Changes in global blocking character in recent decades. *Atmosphere*, **10**, 92, https://doi.org/10.3390/atmos10020092.

Luterbacher, J., D. Dietrich, E. Xoplaki, M. Grosjean, and H. Wanner, 2004: European seasonal and annual temperature variability, trends, and extremes since 1500. *Science*, **303**, 1499–1503, https://doi.org/10.1126/science.1093877.

Matsueda, M., 2011: Predictability of Euro-Russian blocking in summer of 2010. *Geophys. Res. Lett.*, **38**, L06801, https://doi.org/10.1029/2010GL046557.

Meehl, G. A., and C. Tebaldi, 2004: More intense, more frequent, and longer lasting heat waves in the 21st century. *Science*, **305**, 994–997, https://doi.org/10.1126/science.1098704.

Meng, C., Y. Xu, Q. Li, Y. Ma, Q. Feng, W. Ma, J. Pan, and K. Li, 2020: Analyses of observed features and future trend of extreme temperature events in Inner Mongolia of China. *Theor. Appl. Climatol.*, **139**, 577–597, https://doi.org/10.1007/s00704-019-02969-8.

Miguez-Macho, G., G. L. Stenchikov, and A. Robock, 2004: Spectral nudging to eliminate the effects of domain position and geometry in regional climate model simulations. *J. Geophys. Res.*, **109**, D13104, https://doi.org/10.1029/2003JD004495.

Min, K. H., C. H. Chung, J. H. Bae, and D. H. Cha, 2020: Synoptic characteristics of extreme heatwaves over the Korean

Peninsula based on ERA Interim reanalysis data. *Int. J. Climatol.*, **40**, 3179–3195, https://doi.org/10.1002/joc.6390.

Min, S.-K., Y.-H. Kim, S.-M. Lee, S. Sparrow, S. Li, F. C. Lott, and P. A. Stott, 2020: Quantifying human impact on the 2018 summer longest heat wave in South Korea [in "Explaining Extreme Events of 2018 from a Climate Perspective"]. *Bull. Amer. Meteor. Soc.*, **101** (1), S103–S108, https://doi.org/10.1175/BAMS-D-19-0151.1.

Mokhov, I., and A. Timazhev, 2019: Atmospheric blocking and changes in its frequency in the 21st century simulated with the ensemble of climate models. *Russ. Meteor. Hydrol.*, **44**, 369–377, https://doi.org/10.3103/S1068373919060013.

Moon, J., D. H. Cha, M. Lee, and J. Kim, 2018: Impact of spectral nudging on real-time tropical cyclone forecast. *J. Geophys. Res. Atmos.*, **123**, 12 647–12 660, https://doi.org/10.1029/2018JD028550.

Nakai, S., T. Itoh, and T. Morimoto, 1999: Deaths from heat-stroke in Japan: 1968–1994. *Int. J. Biometeor.*, **43**, 124–127, https://doi.org/10.1007/s004840050127.

Perkins, S. E., and L. V. Alexander, 2013: On the measurement of heat waves. *J. Climate*, **26**, 4500–4517, https://doi.org/10.1175/JCLI-D-12-00383.1.

Rex, D. F., 1950: Blocking action in the middle troposphere and its effect upon regional climate: I. An aerological study of blocking action. *Tellus*, **2**, 196–211, https://doi.org/10.3402/tellusa.v2i3.8546.

Reynolds, R. W., T. M. Smith, C. Liu, D. B. Chelton, K. S. Casey, and M. G. Schlax, 2007: Daily high-resolution-blended analyses for sea surface temperature. *J. Climate*, **20**, 5473–5496, https://doi.org/10.1175/2007JCLI1824.1.

Riboldi, J., C. M. Grams, M. Riemer, and H. M. Archambault, 2019: A phase locking perspective on Rossby wave amplification and atmospheric blocking downstream of recurving western North Pacific tropical cyclones. *Mon. Wea. Rev.*, **147**, 567–589, https://doi.org/10.1175/MWR-D-18-0271.1.

Sato, T., and T. Nakamura, 2019: Intensification of hot Eurasian summers by climate change and land–atmosphere interactions. *Sci. Rep.*, **9**, 10866, https://doi.org/10.1038/s41598-019-47291-5.

Seo, E., and Coauthors, 2019: Impact of soil moisture initialization on boreal summer subseasonal forecasts: Mid-latitude surface air temperature and heat wave events. *Climate Dyn.*, **52**, 1695–1709, https://doi.org/10.1007/s00382-018-4221-4.

——, M.-I. Lee, S. D. Schubert, R. D. Koster, and H. S. Kang, 2020: Investigation of the 2016 Eurasia heat wave as an event of the recent warming. *Environ. Res. Lett.*, **15**, 114018, https://doi.org/10.1088/1748-9326/abbbae.

Skamarock, W. C., J. B. Klemp, J. Dudhia, D. O. Gill, D. M. Barker, W. Wang, and J. G. Powers, 2005: A description of the Advanced Research WRF version 2. NCAR Tech. Note NCAR/TN-468+STR, 88 pp., https://doi.org/10.5065/D6DZ069T.

Son, J.-Y., J.-T. Lee, G. B. Anderson, and M. L. Bell, 2012: The impact of heat waves on mortality in seven major cities in Korea. *Environ. Health Perspect.*, **120**, 566–571, https://doi.org/10.1289/ehp.1103759.

Sun, Y., X. Zhang, F. W. Zwiers, L. Song, H. Wan, T. Hu, H. Yin, and G. Ren, 2014: Rapid increase in the risk of extreme summer heat in eastern China. *Nat. Climate Change*, **4**, 1082–1085, https://doi.org/10.1038/nclimate2410.

Tewari, M., and Coauthors, 2004: Implementation and verification of the unified NOAH land surface model in the WRF Model. *20th Conf. on Weather Analysis and Forecasting/16th Conf. on Numerical Weather Prediction*, Seattle, WA, Amer. Meteor. Soc., 14.2a, https://ams.confex.com/ams/pdfpapers/69061.pdf.

von Storch, H., H. Langenberg, and F. Feser, 2000: A spectral nudging technique for dynamical downscaling purposes. *Mon. Wea. Rev.*, **128**, 3664–3673, https://doi.org/10.1175/1520-0493(2000)128<3664:ASNTFD>2.0.CO;2.

Wang, P., J. Tang, X. Sun, J. Liu, and F. Juan, 2019: Spatiotemporal characteristics of heat waves over China in regional climate simulations within the CORDEX-EA project. *Climate Dyn.*, **52**, 799–818, https://doi.org/10.1007/s00382-018-4167-6.

Xu, K., R. Lu, B.-J. Kim, J.-K. Park, J. Mao, J.-Y. Byon, R. Chen, and E.-B. Kim, 2019: Large-scale circulation anomalies associated with extreme heat in South Korea and southern–central Japan. *J. Climate*, **32**, 2747–2759, https://doi.org/10.1175/JCLI-D-18-0485.1.

Xue, Y., F. J. Zeng, K. E. Mitchell, Z. Janjić, and E. Rogers, 2001: The impact of land surface processes on simulations of the U.S. hydrological cycle: A case study of the 1993 flood using the SSiB land surface model in the NCEP Eta regional model. *Mon. Wea. Rev.*, **129**, 2833–2860, https://doi.org/10.1175/1520-0493(2001)129<2833:TIOLSP>2.0.CO;2.

Yeh, S.-W., Y.-J. Won, J.-S. Hong, K.-J. Lee, M. Kwon, K.-H. Seo, and Y.-G. Ham, 2018: The record-breaking heat wave in 2016 over South Korea and its physical mechanism. *Mon. Wea. Rev.*, **146**, 1463–1474, https://doi.org/10.1175/MWR-D-17-0205.1.

Yeo, S. R., S. W. Yeh, and W. S. Lee, 2019: Two types of heat wave in Korea associated with atmospheric circulation pattern. *J. Geophys. Res. Atmos.*, **124**, 7498–7511, https://doi.org/10.1029/2018JD030170.

Yoon, D., D.-H. Cha, G. Lee, C. Park, M. I. Lee, and K. H. Min, 2018: Impacts of synoptic and local factors on heat wave events over southeastern region of Korea in 2015. *J. Geophys. Res. Atmos.*, **123**, 12 081–12 096, https://doi.org/10.1029/2018JD029247.

——, ——, M.-I. Lee, K.-H. Min, J. Kim, S.-Y. Jun, and Y. Choi, 2020: Recent changes in heatwave characteristics over Korea. *Climate Dyn.*, **55**, 1685–1696, https://doi.org/10.1007/s00382-020-05420-1.

Zhang, P., and Coauthors, 2020: Abrupt shift to hotter and drier climate over inner East Asia beyond the tipping point. *Science*, **370**, 1095–1099, https://doi.org/10.1126/science.abb3368.